Supporting Information

Vacancy-Mediated Dual-Step Phosphorization-Sulfurization of $MnMoO_4$ for Efficient Acidic Hydrogen Evolution

Jyoti Ganapati Badiger[a], Chae-Eun Lim[b], Fawad Tariq[c], Maheswari Arunachalam[d], Suzan Abdelfattah Sayed[e], Alaa M. Ibrahim[a], Sang-Wan Ryu[c], Byung-Hyun Kim[b,*], Soon Hyung Kang[d,*]

[a]*Department of Interdisciplinary Program for Photonic Engineering, Chonnam National University, Gwangju 61186, Republic of Korea*
[b]*Department of Applied Chemistry, Center for Bionano Intelligence Education and Research, Hanyang University, ERICA, Ansan, 15588, Republic of Korea*
[c]*Department of Physics, Chonnam National University, Gwangju 61186, Republic of Korea*
[d]*Department of Chemistry Education and Optoelectronic Convergence Research Center, Chonnam National University, Gwangju 61186, Republic of Korea*
[e]*Department of Chemical Engineering, Chonnam National University, Gwangju 61186, Republic of Korea*

[*]E-mail: bkkim00@hanyang.ac.kr (Byung-Hyun Kim), skang@jnu.ac.kr (Soon Hyung Kang)

Experimental Details

Mass activity

Mass activity is an important quantitative parameter used to evaluate the intrinsic catalytic performance of an electrocatalyst, as it normalizes the catalytic current to the amount of catalyst loaded on the electrode [1]. It reflects how efficiently the catalyst mass contributes to the electrochemical reaction.

The mass activity was calculated by normalizing the measured current density to the catalyst loading according to the following equation [1]:

$$\text{Mass activity} = \frac{j}{M}(mA \cdot mg^{-1}), \quad \cdots\cdots [1]$$

where j is the current density shown in the HER polarization curves, and M is the mass of catalyst loading.

Turnover frequency (TOF)

Turnover frequency (TOF) is another key parameter for evaluating electrocatalytic activity at different overpotentials. It represents the number of hydrogen (or oxygen) molecules generated per active site per unit time and provides insight into the intrinsic catalytic efficiency [2]. The following equation is used to estimate the TOF at different overpotentials.

$$TOF = \frac{jA}{nFm}(s^{-1}), \quad \cdots\cdots [2]$$

where j is the current density ($mA \cdot cm^{-2}$) observed in the HER polarization curves, A is the surface area of the electrode (cm^2), n is the number (2) of electrons for the HER, F is the Faradaic constant (96485 C/mol), and m is the number of moles of the loaded catalyst.

Figures & Tables

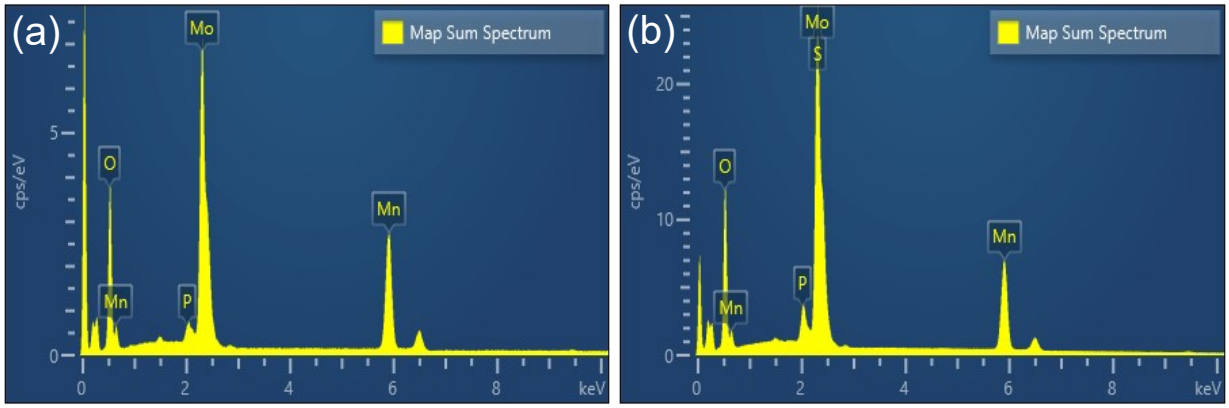

Figure S1. EDS analysis of (a) P-MnMoO4 and (b) P, S-$MnMoO_4$ electrocatalysts.

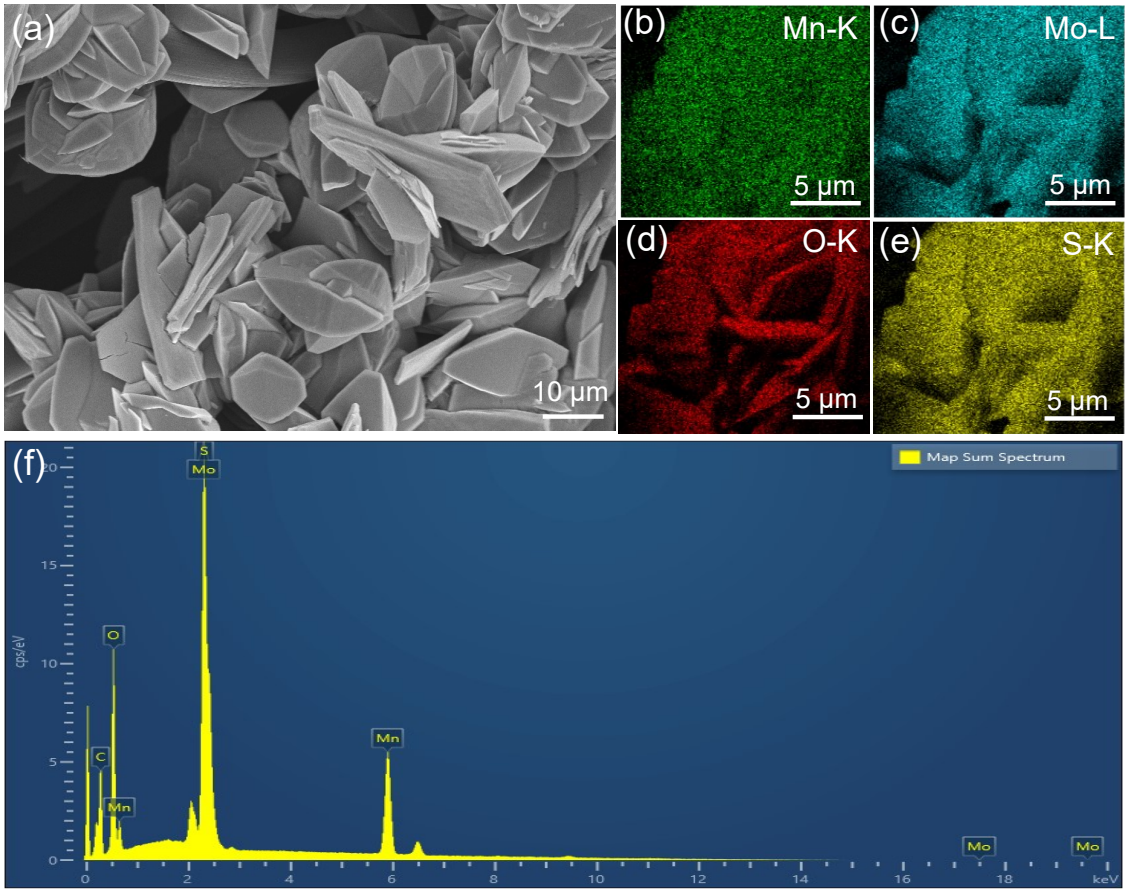

Figure S2. (a) FE-SEM image, (b-e) corresponding elemental mapping and (f) EDS spectra of S-$MnMoO_4$ without intermediate phosphorization.

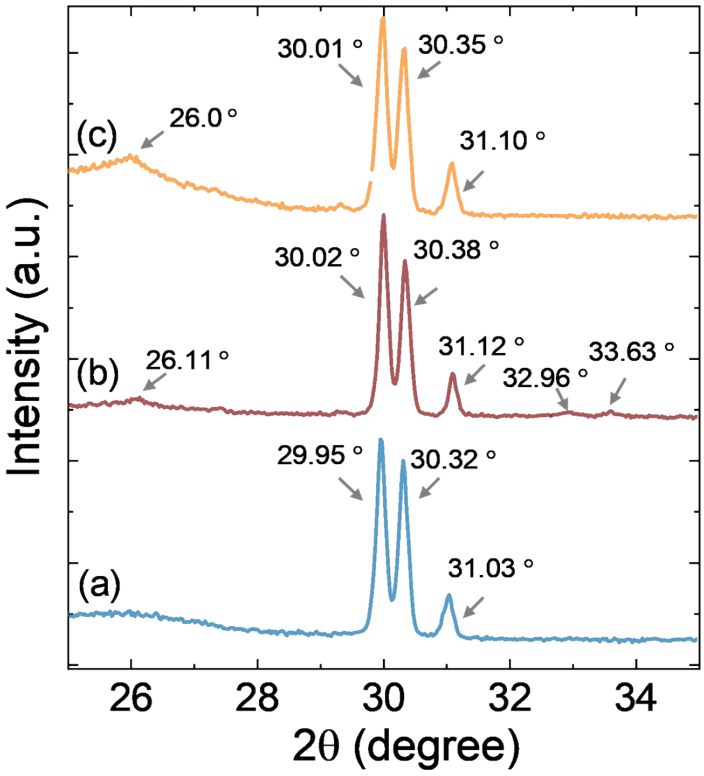

Figure S3. Magnified XRD pattern of (a) $MnMoO_4$, (b) P- $MnMoO_4$, and (c) P,S- $MnMoO_4$ electrocatalysts.

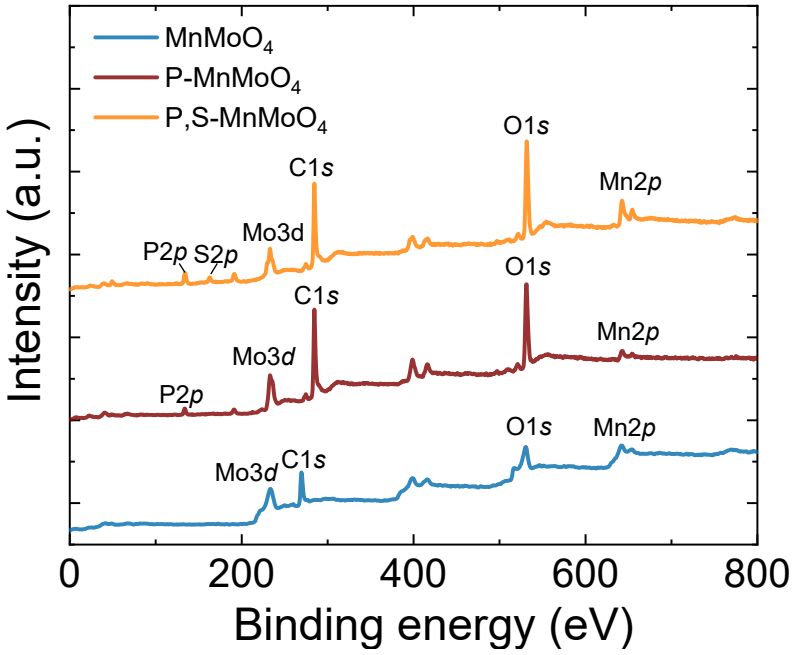

Figure S4. Wide-scan XPS spectra of $MnMoO_4$, P-$MnMoO_4$ and P,S-$MnMoO_4$ electrocatalysts.

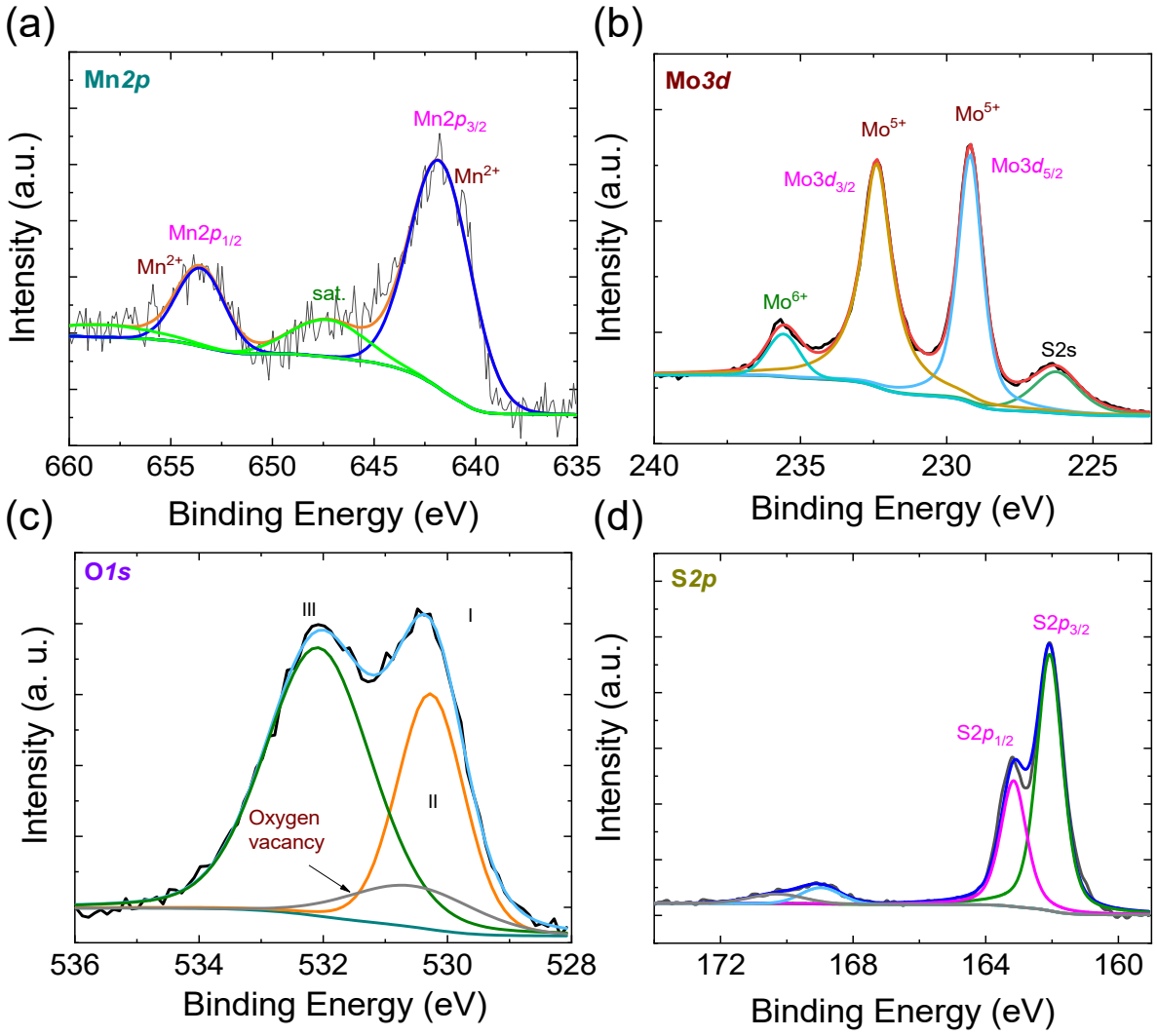

Figure S5. High-resolution core-level XPS spectra of S-$MnMoO_4$ electrocatalyst: (a) Mn*2p*, (b) Mo*3d*, (c) O*1s*, and (d) S*2p*.

Table S1. XPS-derived binding energy peak positions.

Peak	Component	Peak position (eV)		
		$MnMoO_4$	**P-$MnMoO_4$**	**P, S-$MnMoO_4$**
Mn2*p*	Mn2$p_{3/2}$ (Component I)	640.95	642.46	642.58
	Mn2$p_{3/2}$ (Component II)	643.53	-	-
	Mn2$p_{31/2}$ (Component I)	651.97	654.41	654.56
	Mn2$p_{31/2}$ (Component II)	655.44	-	-
Mo3*d*	Mo3$d_{5/2}$ (Component I)	230.79	-	229.17
	Mo3$d_{5/2}$ (Component II)	233.34	233.1	231.79
	Mo3$d_{3/2}$ (Component I)	235.52	-	233.27
	Mo3$d_{3/2}$ (Component II)	237.52	236.13	236.17
O1*s*	Peak I	529.23	530.70	530.68
	Peak II	530.50	531.05	531.11
	Peak III	531.76	532.50	532.57
P2*p*	P2$p_{3/2}$	-	133.15	133.31
	P2$p_{1/2}$	-	134.05	134.21
S2*p*	S2$p_{3/2}$	-	-	161.84
	S2$p_{1/2}$	-	-	163.10

Table S2. Quantification of oxygen vacancies from XPS analysis

Sample	**Peak I**	**Peak II**	**Peak III**	**Total area**	**Related defect-related O (%)***
$MnMoO_4$	63760.63	16488.82	8597.60	88847.05	18.56
P-$MnMoO_4$	24238.93	42862.83	29090.67	97191.76	44.10
P, S-$MnMoO_4$	24086.11	36924.54	27774.55	88785.2	41.59

*Calculated as (Peak II area / Total O1*s* area) × 100.

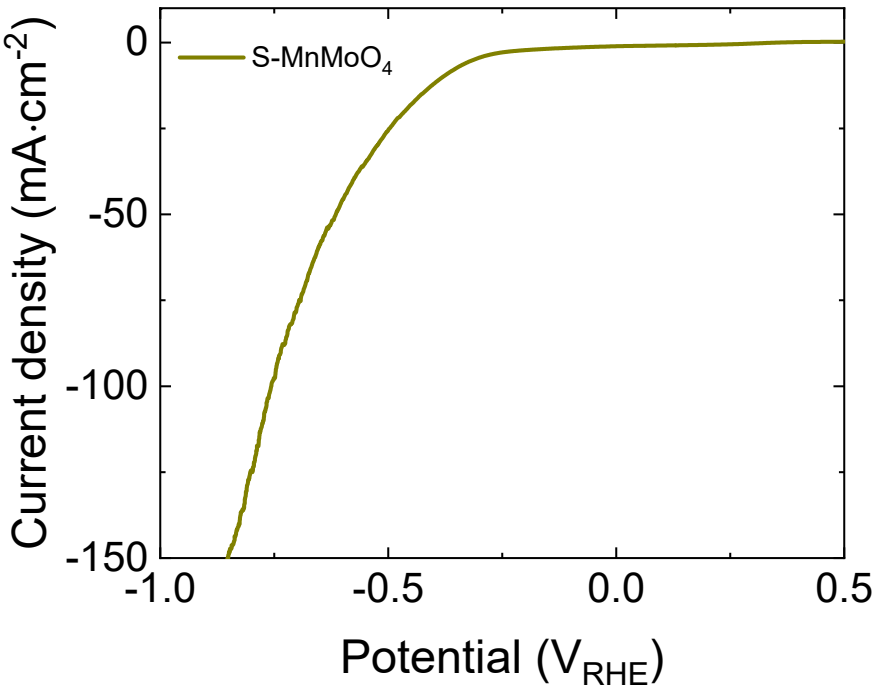

Figure S6. Polarization curve for S-$MnMoO_4$ electrocatalysts without phosphorization.

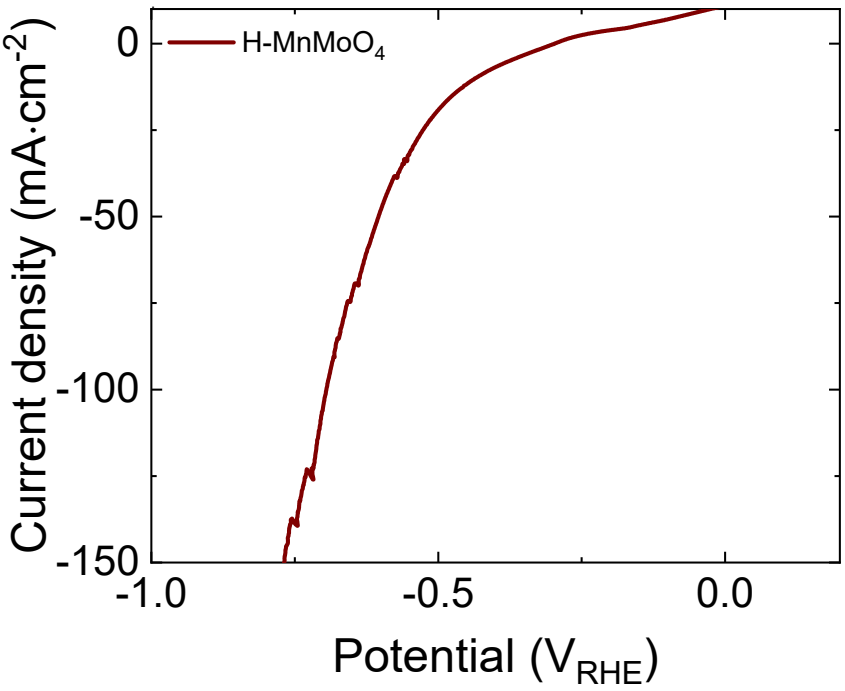

Figure S7. Polarization curve of H-$MnMoO_4$ electrocatalyst.

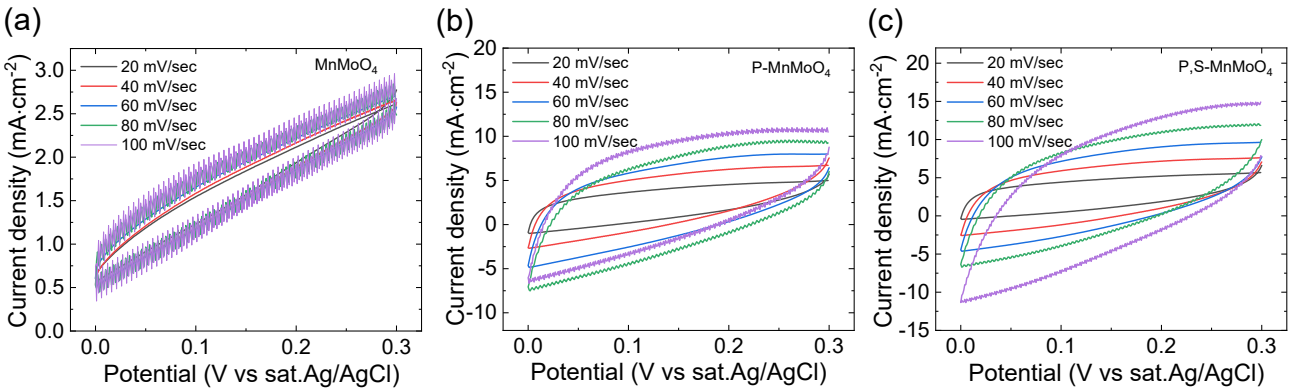

Figure S8. CV curves obtained at scan rates of 20-100 $mV \cdot s^{-1}$ of the (a) $MnMoO_4$, (b) P-$MnMoO_4$ and (c) P,S-$MnMoO_4$ electrocatalysts.

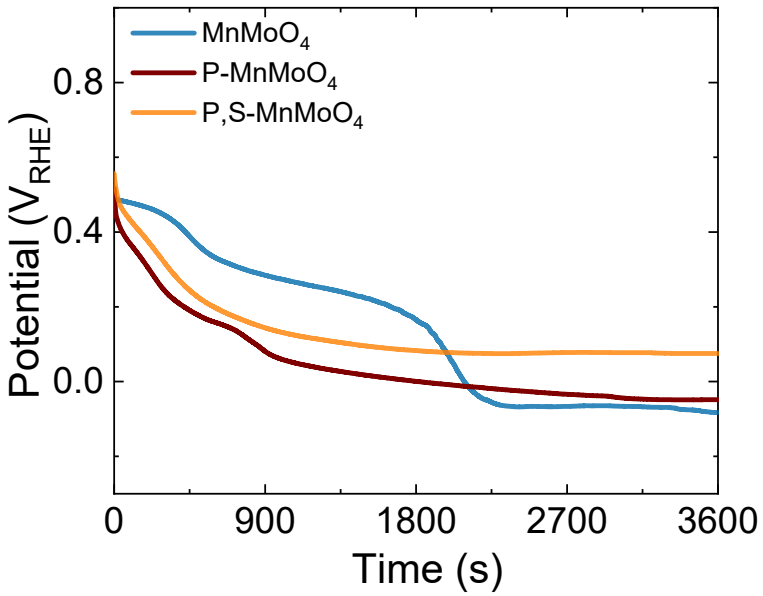

Figure S9. The OCP profile of $MnMoO_4$, P-$MnMoO_4$ and P,S-$MnMoO_4$.

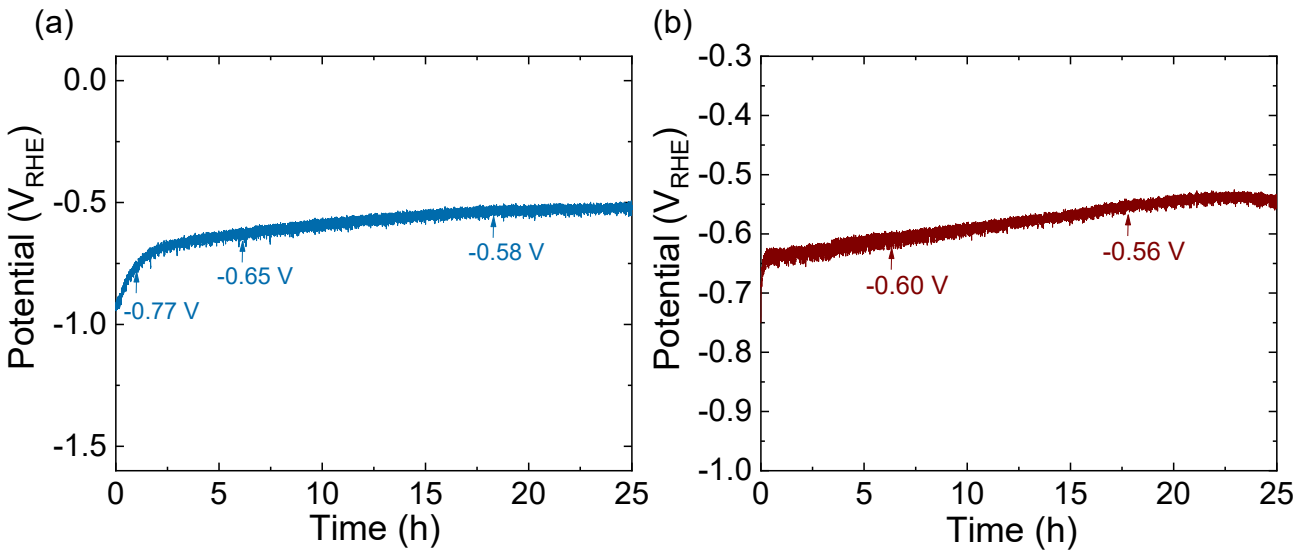

Figure S10. Time-dependent chronopotentiometric stability of (a) $MnMoO_4$, and (b) P-$MnMoO_4$ at the current density of 50 mA·cm^{-2}.

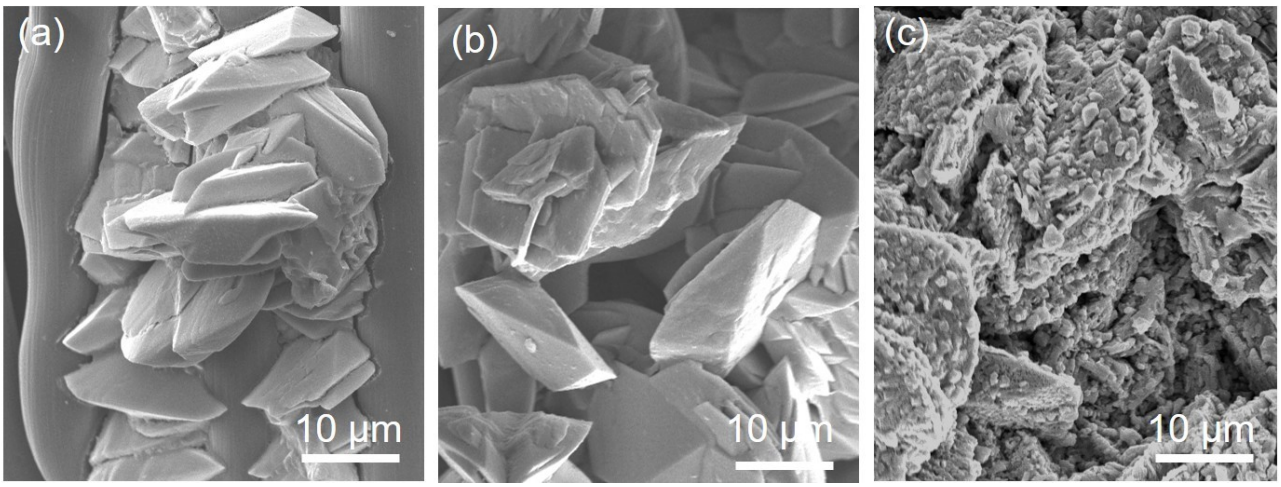

Figure S11. After stability FE-SEM images of (a) $MnMoO_4$, (b) P-$MnMoO_4$, and (c) P,S-$MnMoO_4$ at 10 $mA \cdot cm^{-2}$ of current density

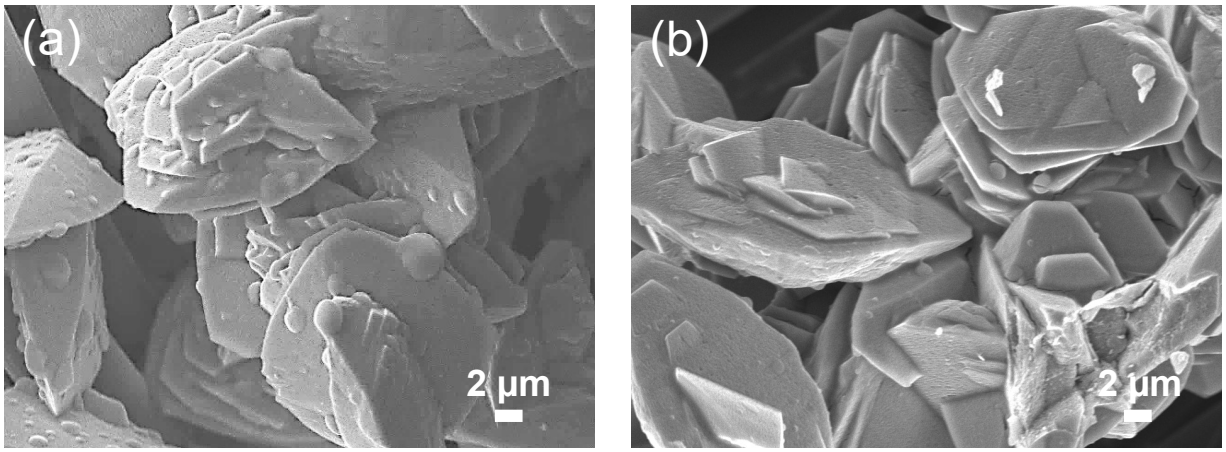

Figure S12. After stability FE-SEM images of P,S-$MnMoO_4$ at (a) 50 mA·cm^{-2} and (b) 100 mA·cm^{-2} of current density.

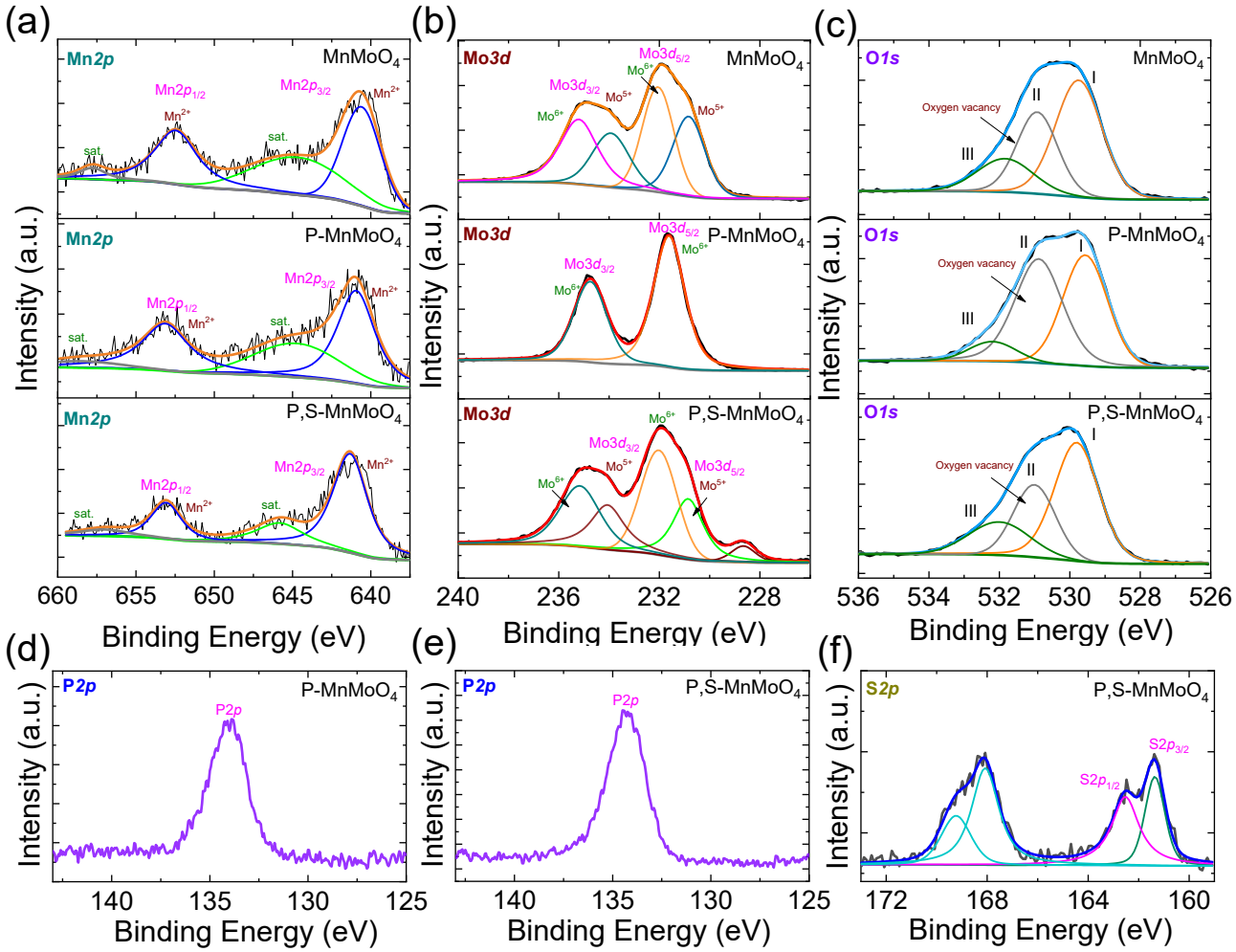

Figure S13. After stability High-resolution core-level XPS spectra of MnMoO4-based electrocatalysts: (a) Mn2*p*, (b) Mo3*d*, (C) O1*s* spectra of $MnMoO_4$, P-$MnMoO_4$ and P,S-$MnMoO_4$; (d,e) P2*p* spectra of P-$MnMoO_4$ and P,S-$MnMoO_4$; and (f) S2*p* spectrum of P, S-$MnMoO_4$.

Table S3. After stability XPS-derived binding energy peak positions of $MnMoO_4$ based electrocatalysts.

Peak	Component	Peak position (eV)		
		$MnMoO_4$	**P-$MnMoO_4$**	**P, S-$MnMoO_4$**
Mn2*p*	Mn2$p_{3/2}$ (Component I)	640.69	640.95	641.38
	Mn2$p_{31/2}$ (Component I)	652.51	653.15	653.02
Mo3*d*	Mo3$d_{5/2}$ (Component I)	230.81	-	230.84
	Mo3$d_{5/2}$ (Component II)	232.09	232	232.02
	Mo3$d_{3/2}$ (Component I)	233.94	-	233.98
	Mo3$d_{3/2}$ (Component II)	235.20	235.02	235.18
O1*s*	Peak I	529.78	529.57	529.82
	Peak II	530.97	530.91	531.03
	Peak III	531.89	532.23	531.99
P2*p*	P2*p*	-	133.95	134.29
S2*p*	S2$p_{3/2}$	-	-	161.36
	S2$p_{1/2}$	-	-	162.55

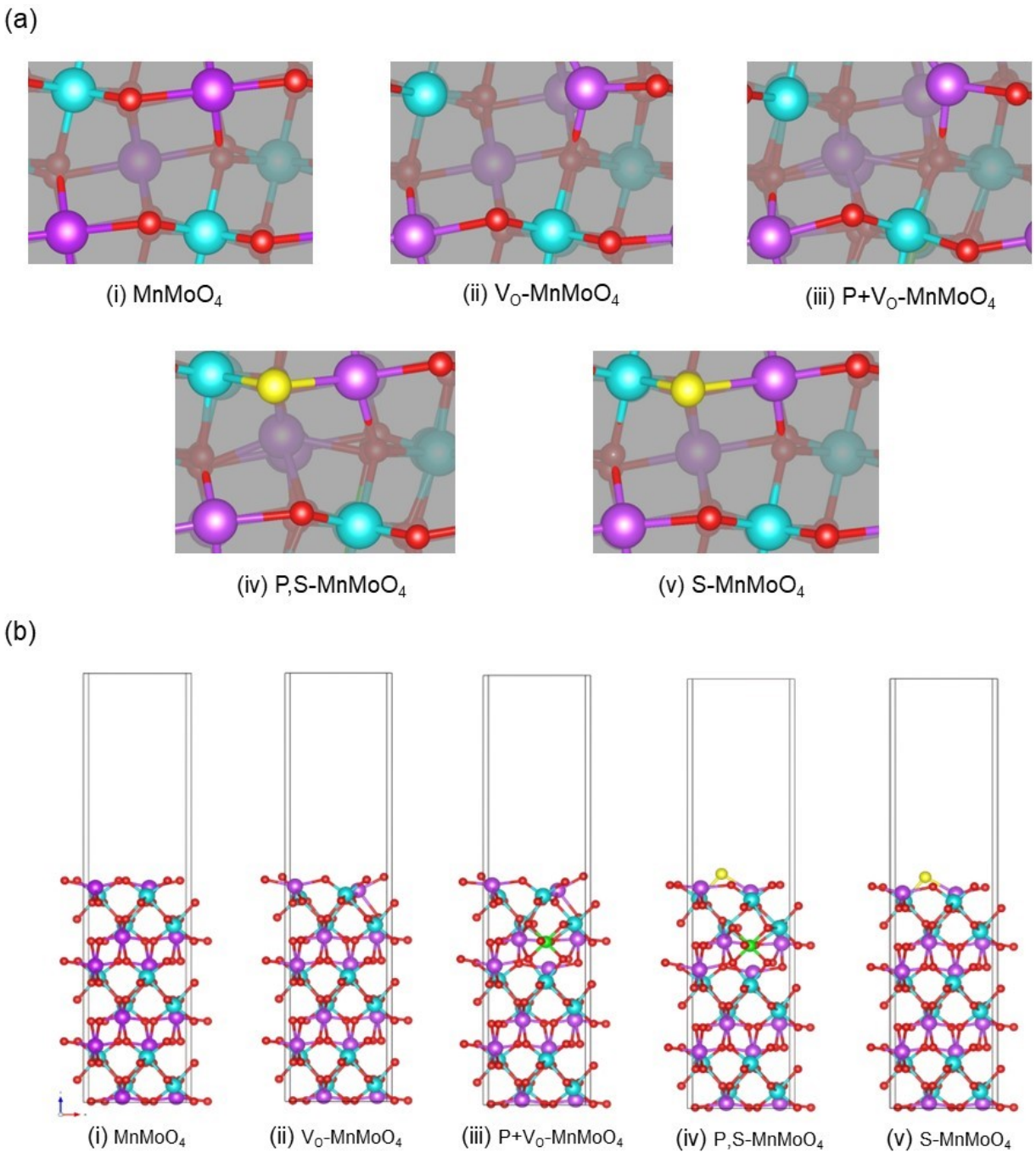

Figure S14. Representative surface models for Pristine $MnMoO_4$, Vo-$MnMoO_4$, P+Vo-$MnMoO_4$, P,S-$MnMoO_4$ and S-$MnMoO_4$ electrocatalysts: (a) top view and (b) side view along the *y*-axis.

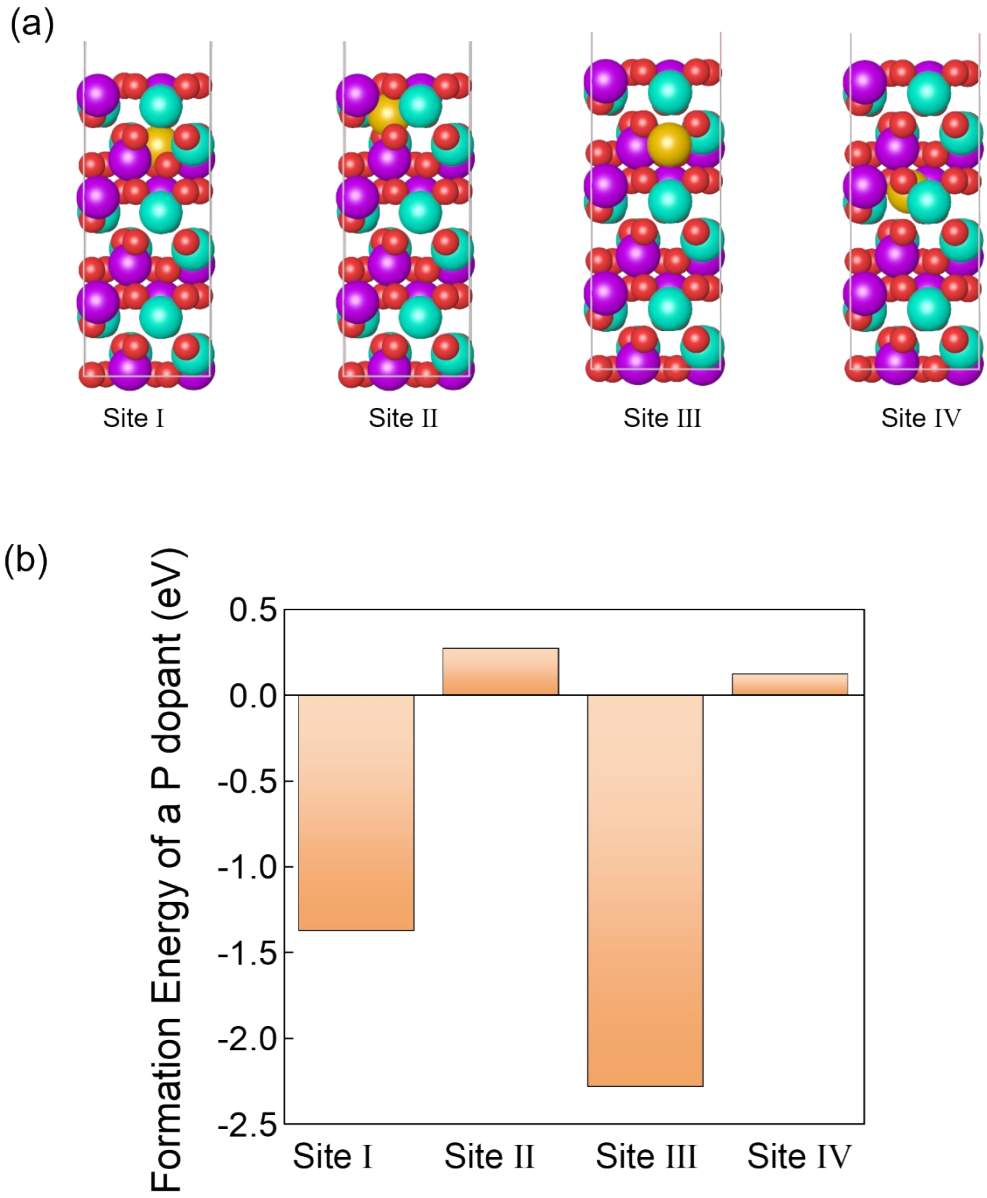

Figure S15. (a) representative atomic configurations of phosphorus-doped pristine $MnMoO_4$ at different interstitial sites (I–IV) and (b) Incorporation formation energies of phosphorus at four distinct interstitial sites.

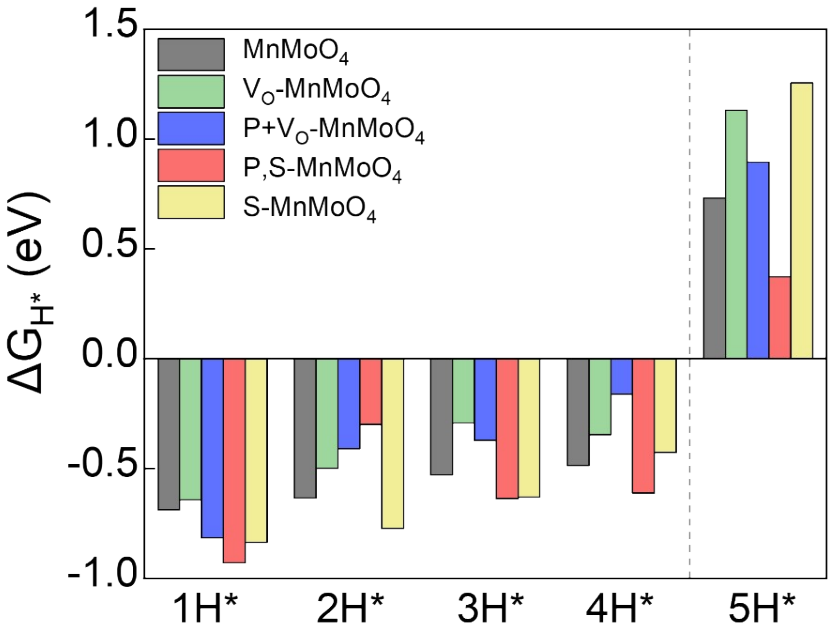

Figure S16. Systematic adsorption calculations by utilizing Gibbs free energy of hydrogen adsorption for prepared electrocatalysts.

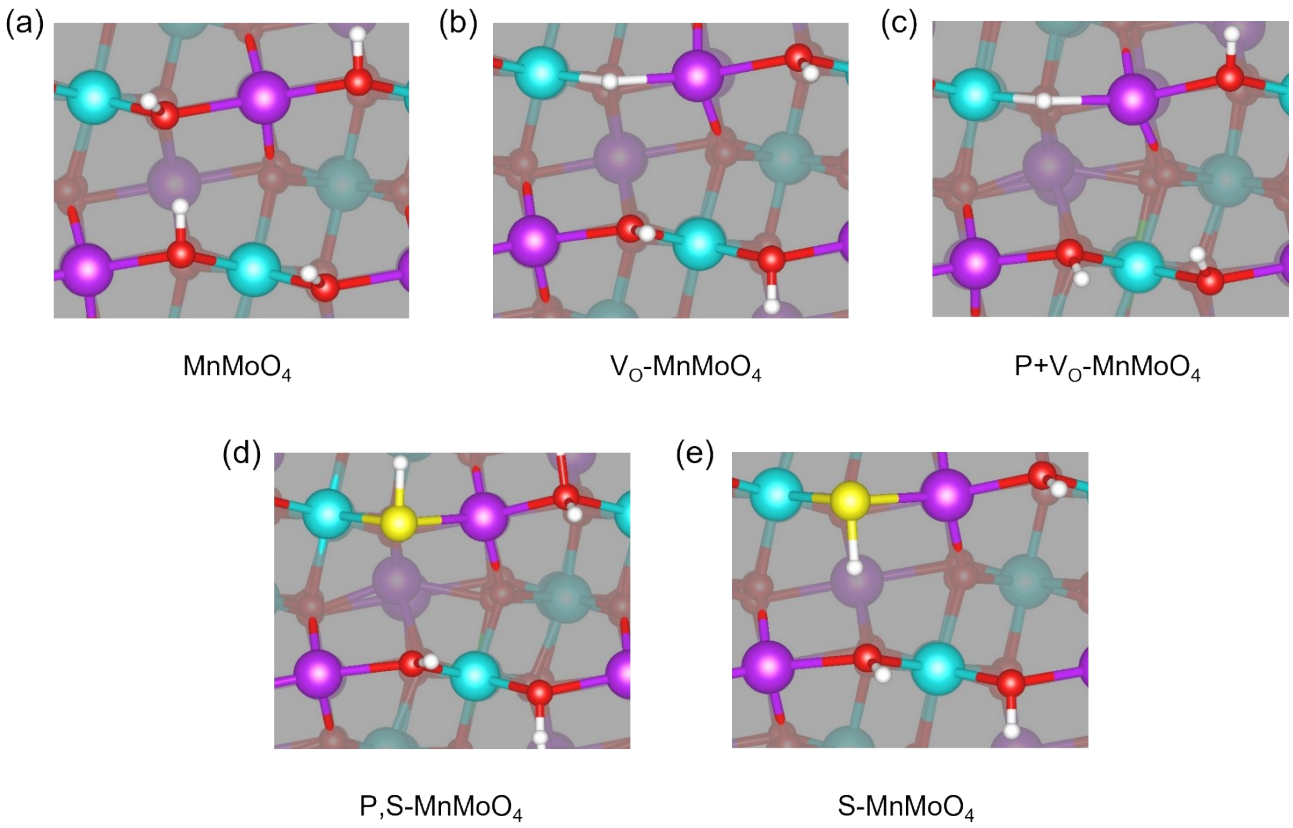

Figure S17. Pre-hydrogenated surface for (a) $MnMoO_4$, (b) Vo-$MnMoO_4$, (c) P+Vo-$MnMoO_4$, (d) P,S-$MnMoO_4$ and (e) S-$MnMoO_4$ electrocatalysts.

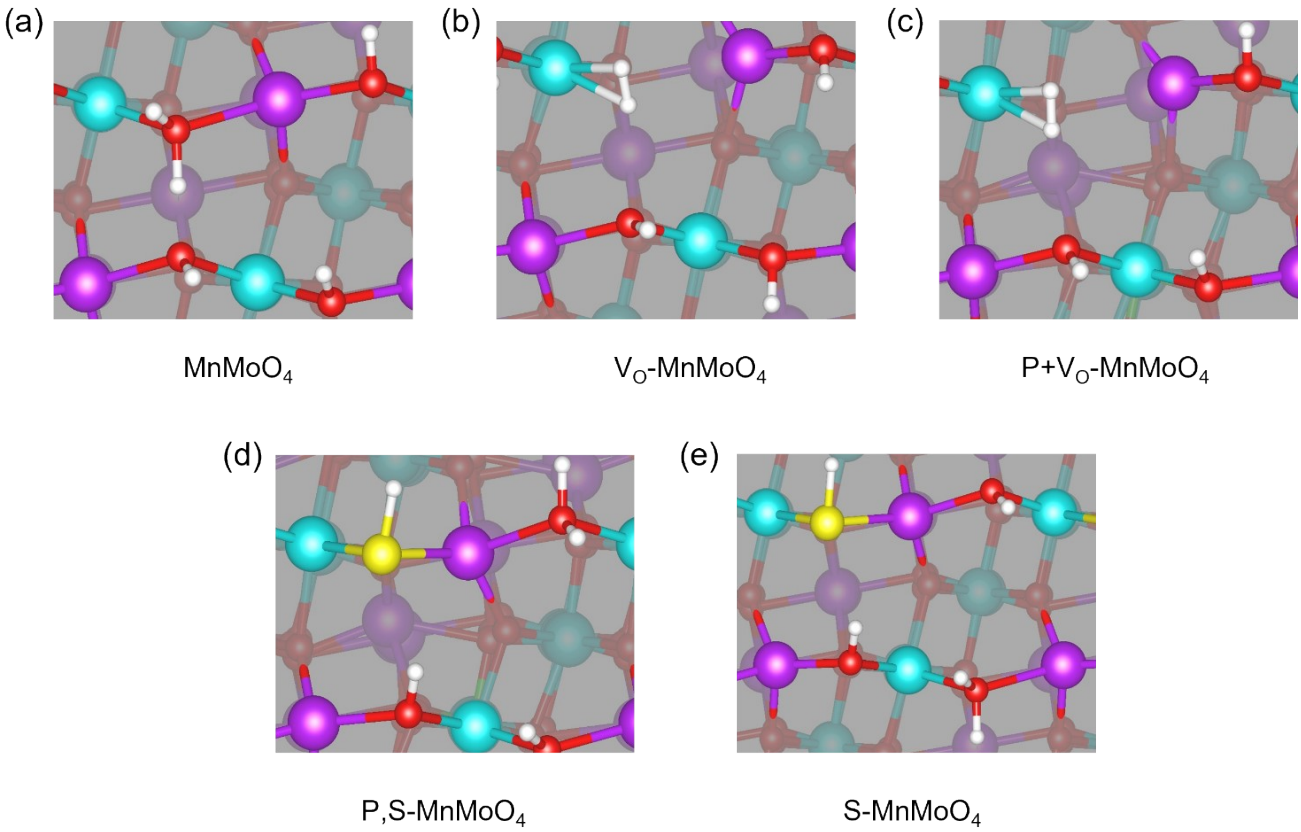

Figure S18. Fifth hydrogen atom ($5H^*$) adsorption of the catalytic turnover involved metal active sites for (a) $MnMoO_4$, (b) Vo-$MnMoO_4$, (c) P+Vo-$MnMoO_4$, (d) P,S-$MnMoO_4$ and (e) S-$MnMoO_4$ electrocatalysts.

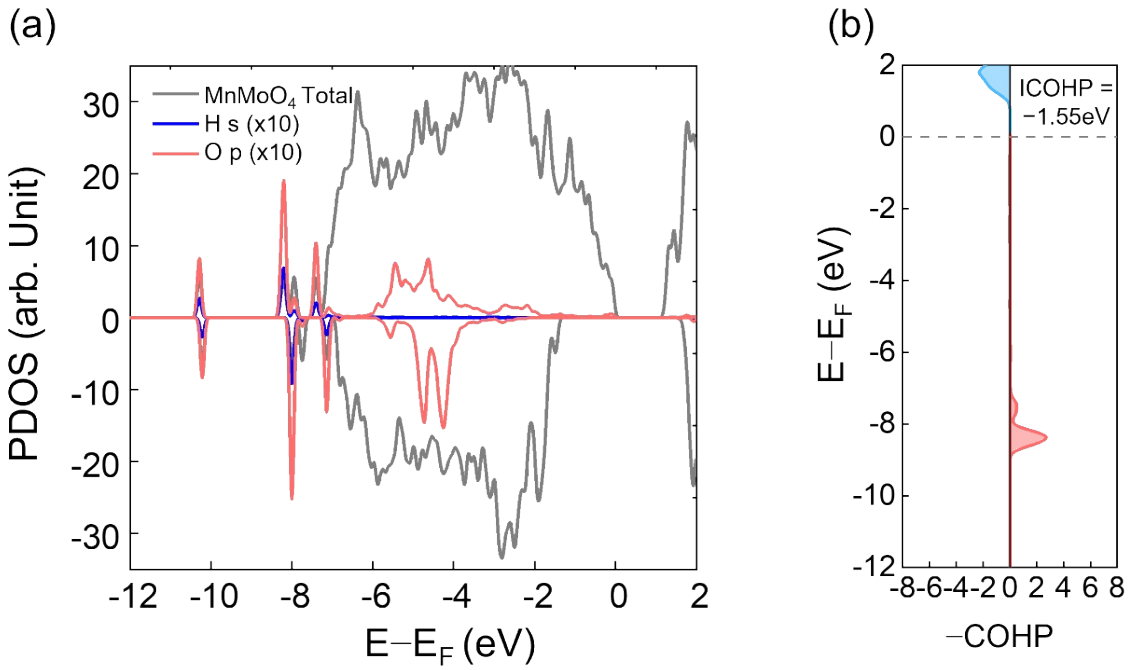

Figure S19. (a) Projected density of states (PDOS) and (b) Crystal orbital Hamilton population (COHP) and integrated COHP (ICOHP) values for pristine $MnMoO_4$

References

1. J. G. Badiger, M. Arunachalam, R. S. Kanase, S. A. Sayed, K.-S. Ahn, J.-S. Ha and S. H. Kang, International Journal of Hydrogen Energy, 2024, 51, 156-168.
2. S. Anantharaj, P. E. Karthik and S. Noda, Angewandte Chemie, 2021, 133, 23235-23251.